Manuscript Number: RSC Advances - RA-ART-12-2023-008676

Entitled "**Tailoring magnetic Sn-MOF for efficient amoxicillin antibiotic removal through process optimization**" Journal of RSC Advances.

1. Material and methods

1.1. Materials

Tin chloride, $FeCl_3.6H_2O$, ethylene glycol, 2-methylimidazole (Hmim) and anhydrous methanol, $SnCl_2$ exactly as they were supplied, they were put to use. Sigma-Aldrich supplied the additional chemicals needed for this study.

1.2. Instruments

A Nicolet IS10 Fourier transform infrared (FTIR) spectrometer (Thermo Fisher Scientific, Waltham, MA, USA) that was equipped with an attenuated total reflectance accessory and which ran in the 4000-400 cm^{-1} range was used to gather FTIR spectra., which was carried out in the temperature range 30-800 °C at a scanning rate of 15 °C min^{-1} and in a nitrogen atmosphere (flow rate 20 mL min–1). X-ray diffraction (XRD) patterns were captured from powder samples through the use of a Siemens diffractometer (model D500, Germany) that was fitted with a Cu-K radiation source (wavelength 1.54 Angstroms (Å)) operating at 30kV and 20 mA. A scanning range of 10-50° and a scanning speed of 5° min^{-1} were used to obtain XRD patterns. The morphology of the investigated sorbents was analysed with the use of a scanning electron microscope (JSM-6510LV, JEOL Ltd., Tokyo, Japan),. A Quantachrome NOVA 3200e (Quantachrome Instruments, Anton Paar Quanta Tec, Inc., Boynton Beach, FL, USA) was utilised for surface and pore analysis (Brunauer Emmett-Teller (BET) surface area, porous volume, and pore size), and NovaWin Software (v11.0) was used for data interpretation. The BET surface area of MTM adsorbents was obtained by the application of nitrogen adsorption-desorption isotherms at 77K through the use of a specific analyser (Quadrasorb–EVO, Quantachrome, USA). The surface charge of MSn-MOF adsorbents was measured in the pH range 3.0-10.0 with a Zettaliter Nano instrument (ZS90, Malvern, UK). ultrasonic bath sonicator (Elmasonic P300H ultrasonic bath, continuous mode, power 380 W, Elma Schmidbauer GmbH, Singen, Germany), ultrasonic bath sonicator (Elmasonic P300H ultrasonic bath, continuous mode, power 380 W, Elma Schmidbauer GmbH, Singen, Germany).

Table S1. MSn-MOF crystallographic data.

$2\theta_{Obs.}$ (°)	**$2\theta_{Calc.}$ (°)**	**diff**	**(*hkl*)**
14.796	14.788	0.008	0 2 0
15.76	15.774	0.014	1 1 1
25.088	25.073	0.014	3 2 0
26.88	26.830	0.058	0 4 0
29.796	29.830	-0.034	0 3 1
31.642	31.663	-0.21	1 3 2
56.223	56.164	0.059	0 4 2
61.064	61.064	-0.026	7 2 1
61.714	61.705	0.009	5 1 2

Table S2. Characteristics of the adsorption isotherm for AMX on MSn-MOF.

Models	Adsorption parameter	
Langmuir	$q_{m\ exp}$ (mmol/g)	2.72
	q_m (mmol/g)	2.76
	K_L (L/mmol)	64989.61
	R_L	0.05
	Reduced Chi-Sqr	0.01835
	Residual Sum of Squares	0.29362
	R-Square (COD)	0.97981
	Adj. R-Square	0.97855
	R^2	0.98
Freundlich	n	6.02
	K_F (mmol/g)(L/mmol)$^{1/n}$	0.105
	Reduced Chi-Sqr	0.0138
	Residual Sum of Squares	13.76172
	R-Square (COD)	0.79678
	Adj. R-Square	0.79657

	R^2	0.81
Dubinin–Radushkevich	Q_{DR}	3.82
	$K_{DR}(J^2/mol^2)$	9.73572E-10
	Ea (kJ/mol)	20.62
	Reduced Chi-Sqr	3.54548E-4
	Residual Sum of Squares	0.35348
	R-Square (COD)	0.99391
	R^2	0.99391
Temkin	b_T (kJ/mol)	9970.00626
	A_T (L/mg)	1.05193E8
	Reduced Chi-Sqr	1.20392E-5
	Residual Sum of Squares	0.01202
	R-Square (COD)	0.9998
	R^2	0.9998
Khan	qm($mmol.g^{-1}$)	2.72
	k	95134.11775
	n	0.092
	Reduced Chi-Sqr	0.01447
	Residual Sum of Squares	14.43829
	R-Square (COD)	0.75403
	R2	0.75378
Toth	qm ($mmol.g^{-1}$)	2.72
	k	95134.12
	n	0.99
	Reduced Chi-Sqr	1.118E-31
	Residual Sum of Squares	1.11464E-28
	R-Square (COD)	0.996
	R2	0.998
Jovanovic	qm ($mmol.g^{-1}$)	2.69
	b	-49197.6493
	Reduced Chi-Sqr	0.00583
	Residual Sum of Squares	5.81733
	R-Square (COD)	0.91442
	R^2	0.91433

Table S3. List of abbreviation

Symbol	Definition
q_e	the adsorbed amount of dye at equilibrium concentration (mmol/g)
q_{mL}	the maximum sorption capacity (corresponding to the saturation of the monolayer, (mmol/g)
K_L	Langmuir binding constant which is related to the energy of sorption (L/mmol)
C_e	The equilibrium concentration of dyes in solution
K_F	Freundlich constants related to the sorption capacity (mmol/g^{-1}) (L/mmol)$^{1/n}$
n	intensity
K_{DR}	constant related to the sorption energy (J^2 mol^{-2})
q_{DR}	theoretical saturation capacity (mmol/g)
ε	Polanyi potential (J^2mol^{-2})
R	Gas constant (8.314 Jmol^{-1}K^{-1})
T	Temperature where the adsorption occurs
A_T	Temkin isotherm constant
b_T	Temkin constant in relation to heat of adsorption (J/mol)
q_t	is the amount of dye adsorbed (mmol/g)
K_1	Rate constant for Pseudo first order constant for the adsorption processes (min^{-1})
q_2	Maximum adsorption capacity for pseudo second order
K_2	Rate constant for Pseudo first order constant for the adsorption processes (g mg^{-1}min^{-1})
α	Chemical adsorption rate (mgg^{-1}.min^{-1})
β	Coefficient in relation with extension of covered surface
ΔG^o	Free Gibb's energy
ΔH^o	Enthalpy
ΔS^o	Entropy
Kc	distribution coefficient
C_{eq}	Concentration at equilibrium (mg/L)

Table S4. Different adsorbents' AMX adsorption capacities.

Adsorbent	Adsorption capacity (mg/g)	References
NaOH-activated carbon	571	[1]
Organobentonite	26.18	[2]
Modified MMT K10	647.7	[3]
Saccharomyces cerevisiae	12	[4]
Activated carbon from Arundo donax Linn	345	[5]
MIL-53(Al)	758.5	[6]
Powder activated carbon magnetized by Fe_3O_4 nanoparticles	136.9	[7]
PAC-MP	132	[8]
Magnetic graphene nanoplatelets	106.4	[9]
MSn-MOF	993.8	This work
Sn-MOF	1088	This work

Table S5. Results for AMX's adsorption capacity and response surface central composite design.

Run	Actual variables			Yield (mmol/g)			Internally Studentized Residuals	Externally Studentized Residuals	Leverage
	pH	Time (min.)	Dose (g)	Experimental	Predicted	Residue			
1	7	52.5	0.135	2.08	2.08	0.0000	0.000	0.000	0.200
2	2	52.5	0.02	2.08	2.11	-0.0244	-1.867	-2.439	0.750
3	2	52.5	0.25	1.93	1.91	0.0164	1.254	1.319	0.750
4	7	100	0.25	2.42	2.43	-0.0075	-0.575	-0.546	0.750
5	7	5	0.02	1.29	1.28	0.0075	0.575	0.546	0.750
6	12	52.5	0.02	2.08	2.10	-0.0164	-1.254	-1.319	0.750
7	12	100	0.135	2.48	2.49	-0.0169	-1.292	-1.370	0.750
8	12	5	0.135	1.16	1.15	0.0089	0.679	0.650	0.750
9	7	5	0.25	1.13	1.16	-0.0332	-2.546	-8.660[(2)]	0.750
10	7	52.5	0.135	2.08	2.08	0.0000	0.000	0.000	0.200
11	12	52.5	0.25	1.90	1.87	0.0244	1.867	2.439	0.750

12	7	52.5	0.135	2.08	2.08	0.0000	0.000	0.000	0.200
13	7	52.5	0.135	2.08	2.08	0.0000	0.000	0.000	0.200
14	2	100	0.135	2.52	2.53	-0.0089	-0.679	-0.650	0.750
15	7	52.5	0.135	2.08	2.08	0.0000	0.000	0.000	0.200
16	7	100	0.02	2.76	2.73	0.0332	2.546	8.660[2]	0.750
17	2	5	0.135	1.18	1.16	0.0169	1.292	1.370	0.750

Table S6. Evaluation of variance for the models that were fitted.

Source	Sum of Squares	df	Mean Square	F-value	p-value		Standard Error	95% CI Low	95% CI High
Intercept	2.08						0.0117	2.05	2.11
Model	-0.0122	9	0.4352	639.39	< 0.0001	Significant			
A-pH	0.6768	1	0.0012	1.76	0.2262		0.0092	-0.0340	0.0096
B-time	-0.1043	1	3.66	5382.97	< 0.0001		0.0092	0.6549	0.6986
C-Dose	-0.0058	1	0.0871	127.95	< 0.0001		0.0092	-0.1261	-0.0825
AB	-0.0078	1	0.0001	0.1980	0.6697		0.0130	-0.0367	0.0250
AC	-0.0447	1	0.0002	0.3539	0.5706		0.0130	-0.0386	0.0231
BC	-0.0746	1	0.0080	11.74	0.0110		0.0130	-0.0755	-0.0138
A^2	-0.1720	1	0.0235	34.47	0.0006		0.0127	-0.1047	-0.0446
B^2	-0.0084	1	0.1246	183.05	< 0.0001		0.0127	-0.2021	-0.1420
C^2	2.08	1	0.0003	0.4335	0.5313		0.0127	-0.0384	0.0217
Residual	0.0048	7	0.0007						
Lack of Fit	0.0048	3	0.0016						
Pure Error	0.0000	4	0.0000						
Cor Total	3.92	16							

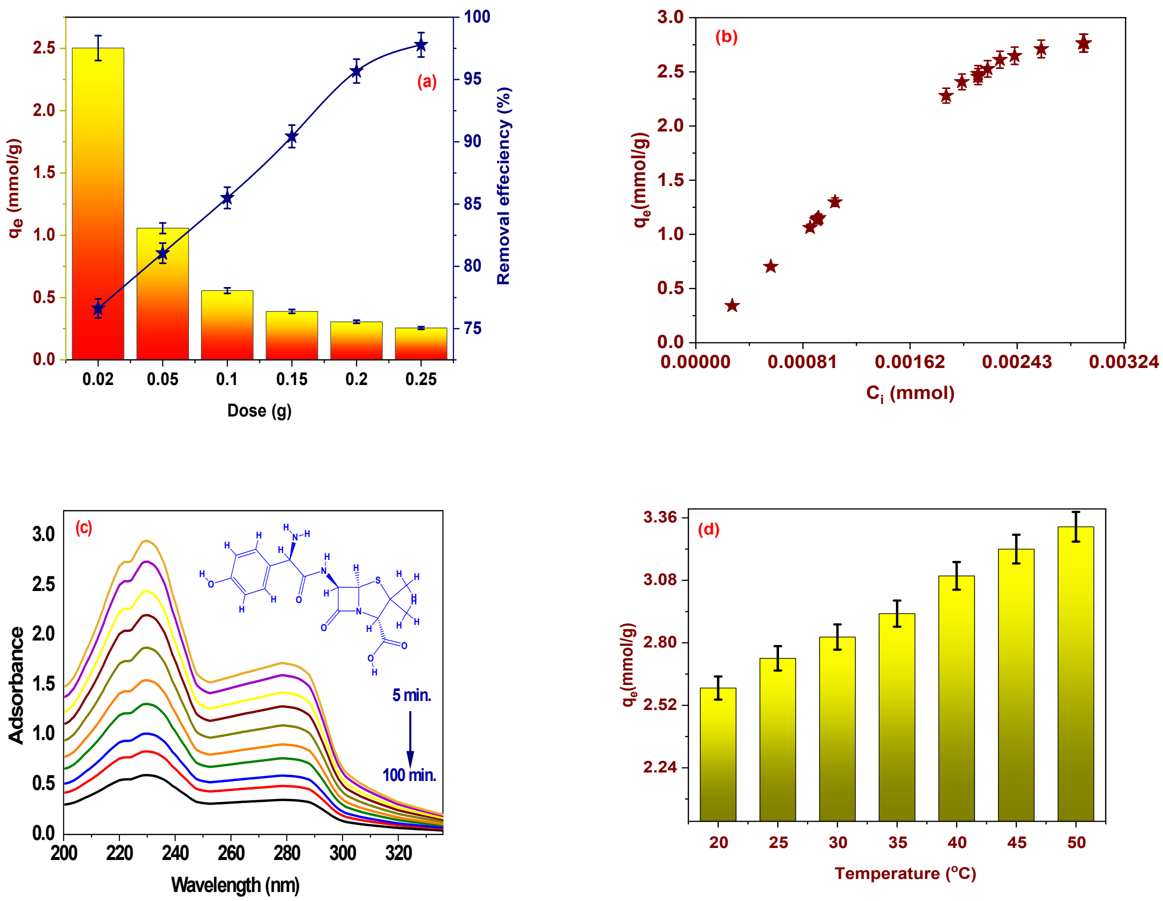

Fig. S1. (a) The effect of dose, (b) effect of initial concentration of AMX, (c) time effect, and (d) temperature effect on adsorption of AMX onto MSn-MOF.

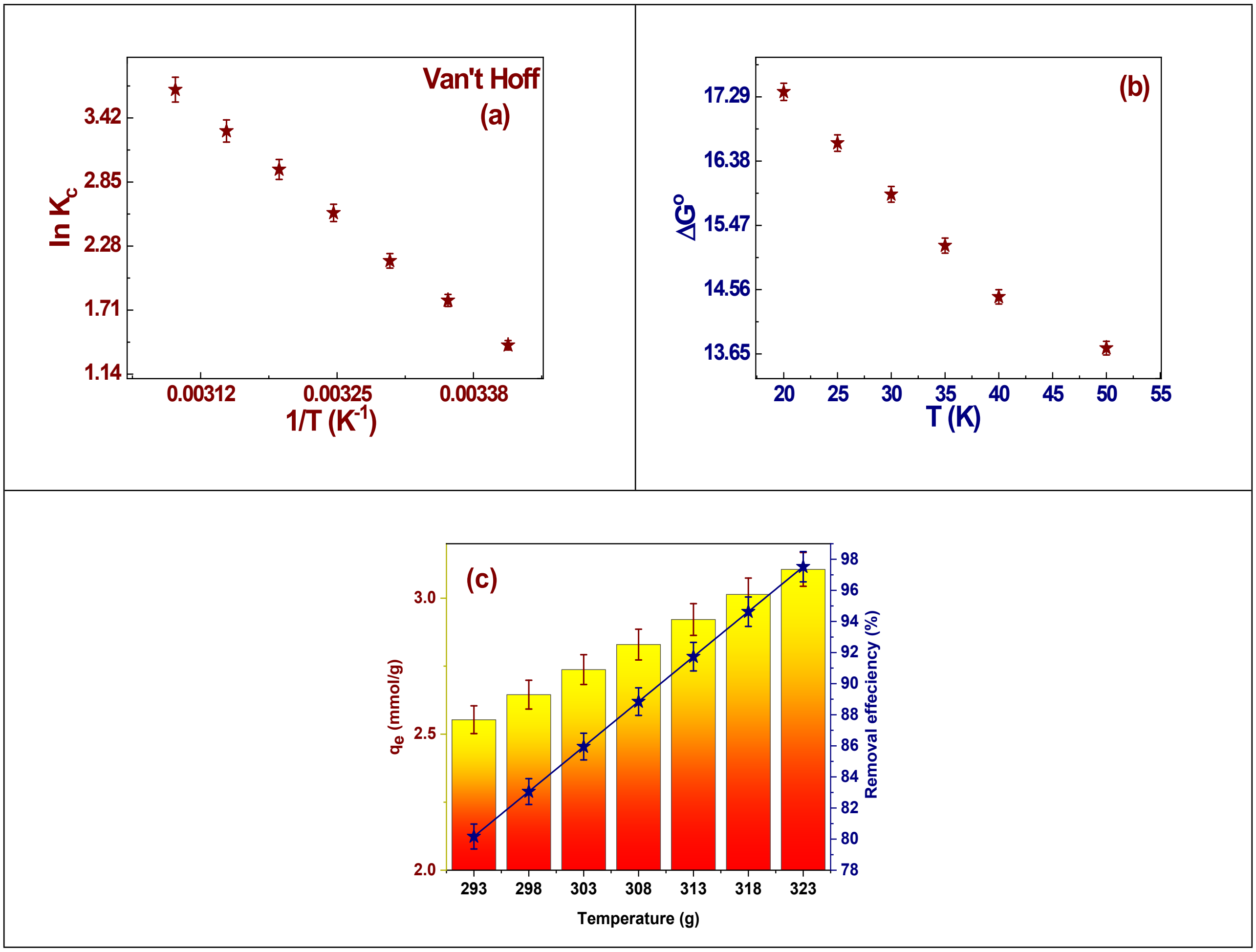

Fig. S2. (a) Van’t Hoff model, (b) Effect of temperature on change on free Gibbs energy, and (c) effect of temperature on adsorption capacity.

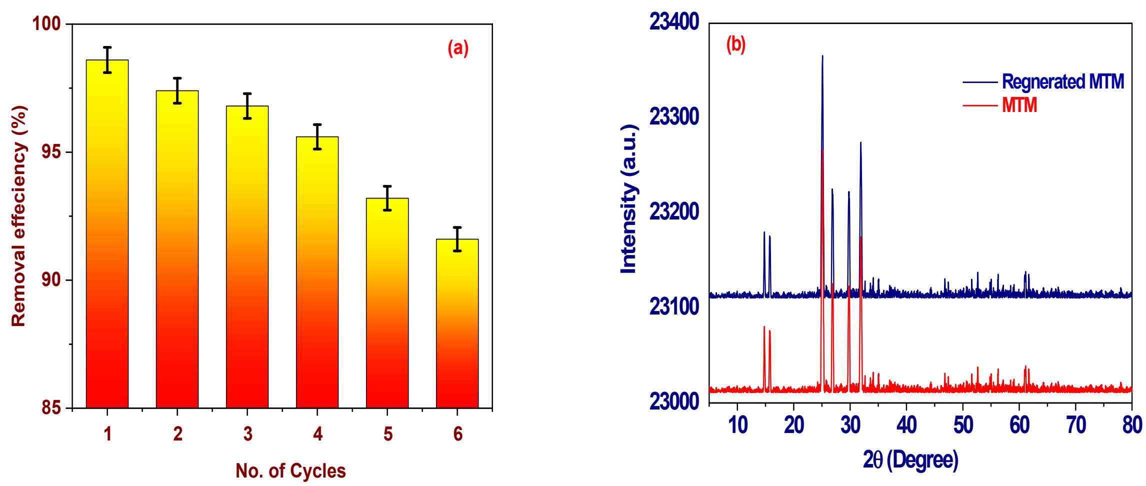

Fig. S3. (a) Reusability efficiency of MSn-MOF, and (b) XRD pattern.

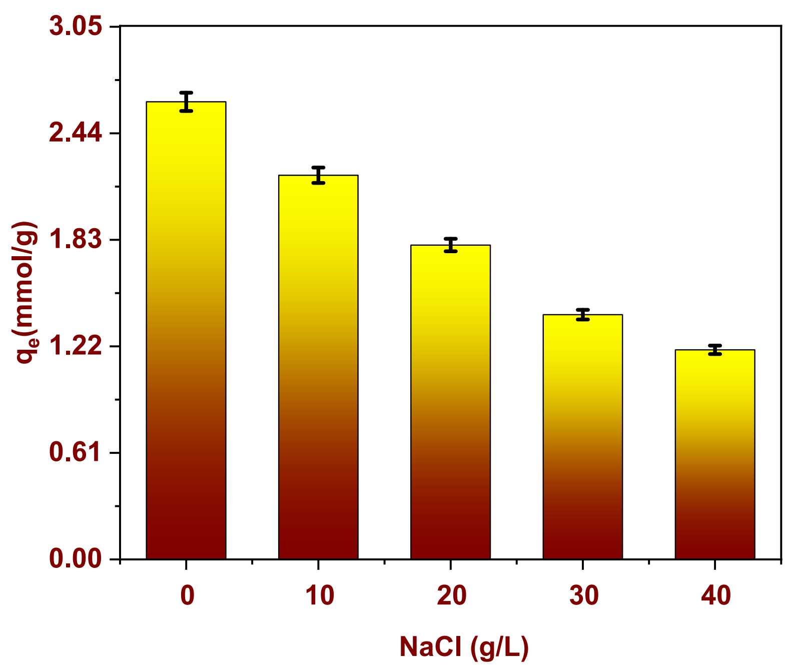

Fig. S4. Effect of interfering ions on adsorption of AMX onto MSn-MOF.

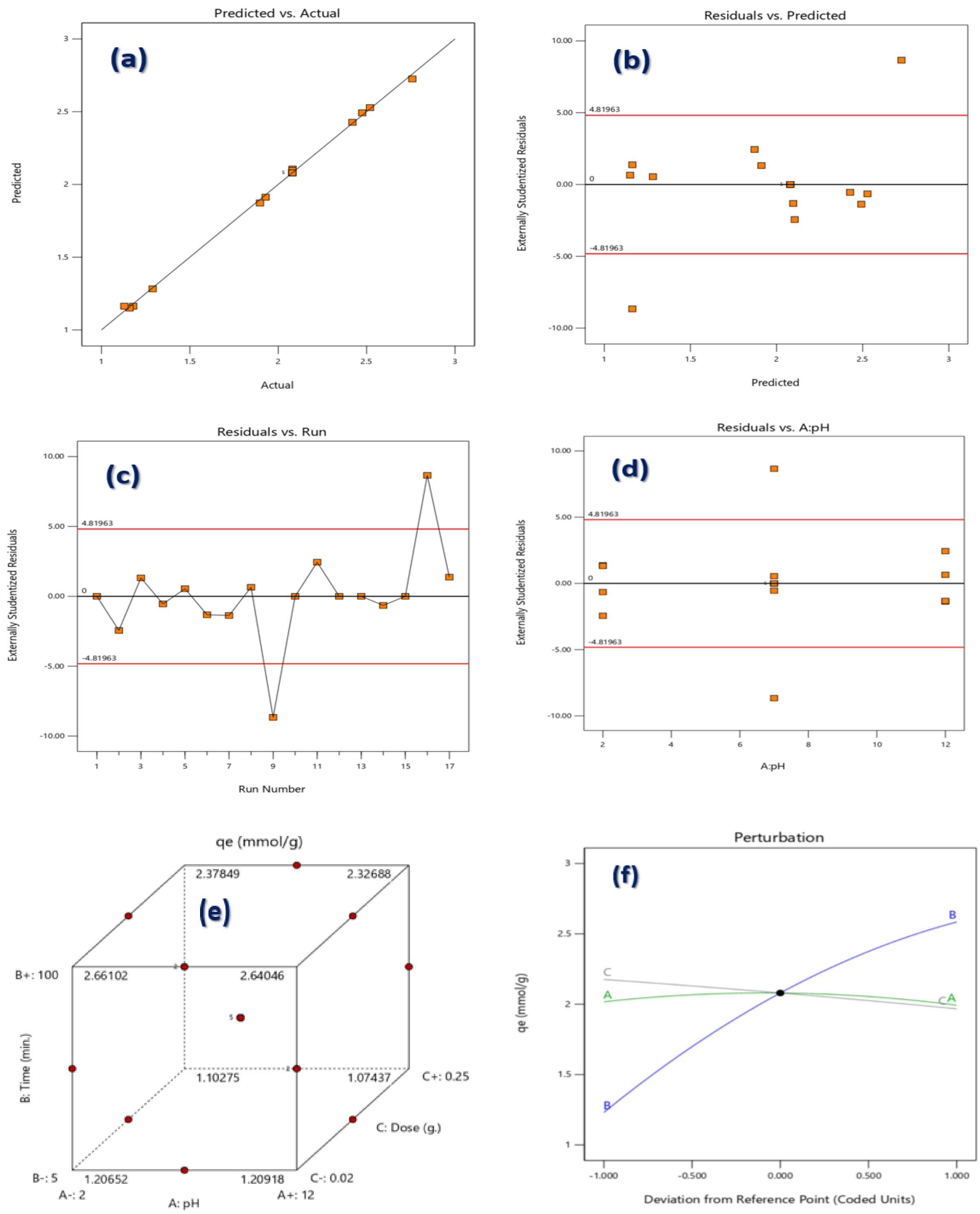

Fig. S5. (a-d) Experimental adsorption capacity *vs.* the predicted adsorption capacity, (e) Graphical optimization of adsorption capacity, and (f) Plot for rate response perturbation.

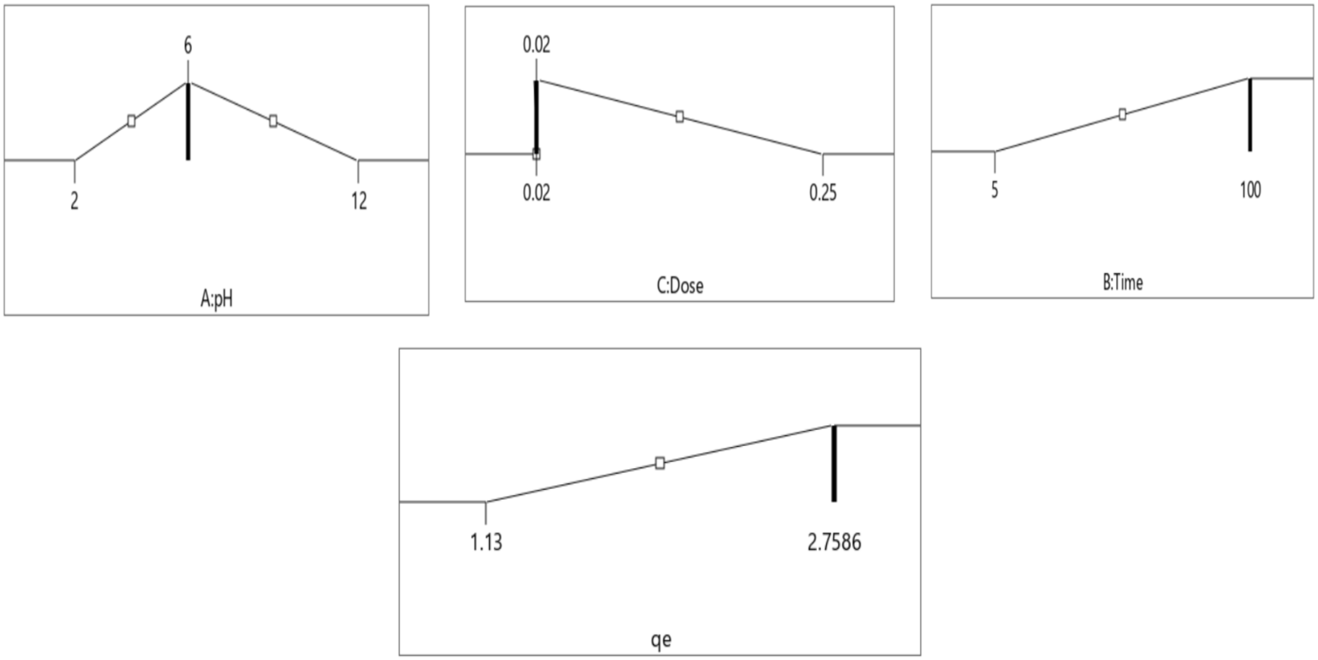

Fig. S6. The removal capacity of AMX is predicted along with its desirability functions.

References

[1] A.L. Cazetta, A.M. Vargas, E.M. Nogami, M.H. Kunita, M.R. Guilherme, A.C. Martins, T.L. Silva, J.C. Moraes, V.C. Almeida, NaOH-activated carbon of high surface area produced from coconut shell: Kinetics and equilibrium studies from the methylene blue adsorption, J Chemical Engineering Journal, 174 (2011) 117-125.

[2] S. xing Zha, Y. Zhou, X. Jin, Z. Chen, The removal of amoxicillin from wastewater using organobentonite, Journal of Environmental Management, 129 (2013) 569-576.

[3] J. Imanipoor, A. Ghafelebashi, M. Mohammadi, M. Dinari, M.R. Ehsani, Fast and effective adsorption of amoxicillin from aqueous solutions by L-methionine modified montmorillonite K10, J Colloids Surfaces A: Physicochemical Engineering Aspects, 611 (2021) 125792.

[4] M.R. Samarghandi, G. Asgari, R. Shokoohi, A. Dargahi, A. Arabkouhsar, Removing amoxicillin antibiotic from aqueous solutions by Saccharomyces cerevisiae bioadsorbent: kinetic, thermodynamic and isotherm studies, J Desalination Water Treat, 152 (2019) 306-315.

[5] M.A. Chayid, M.J. Ahmed, Amoxicillin adsorption on microwave prepared activated carbon from Arundo donax Linn: isotherms, kinetics, and thermodynamics studies, Journal of environmental chemical engineering, 3 (2015) 1592-1601.
[6] J. Imanipoor, M. Mohammadi, M. Dinari, M.R. Ehsani, Adsorption and desorption of amoxicillin antibiotic from water matrices using an effective and recyclable MIL-53 (Al) metal–organic framework adsorbent, Journal of Chemical Engineering Data, 66 (2020) 389-403.
[7] B. Kakavandi, R. Rezaei Kalantary, A. Jonidi Jafari, A. Esrafily, A. Gholizadeh, A. Azari, Efficiency of powder activated carbon magnetized by Fe3O4 nanoparticles for amoxicillin removal from aqueous solutions: Equilibrium and kinetic studies of adsorption process, J Iranian journal of health environment, 7 (2014) 21-34.
[8] H. Liu, Z. Hu, H. Liu, H. Xie, S. Lu, Q. Wang, J. Zhang, Adsorption of amoxicillin by Mn-impregnated activated carbons: performance and mechanisms, J RSC advances, 6 (2016) 11454-11460.
[9] Ö. Kerkez-Kuyumcu, Ş.S. Bayazit, M.A. Salam, Antibiotic amoxicillin removal from aqueous solution using magnetically modified graphene nanoplatelets, Journal of Industrial Engineering Chemistry, 36 (2016) 198-205.